Extrinsic models for the dielectric response of $CaCu_3Ti_4O_{12}$

Morrel H. Cohen, J. B. Neaton, Lixin He, and David Vanderbilt
Department of Physics and Astronomy, Rutgers University,
Piscataway, New Jersey 08855-0849
(April 8, 2003)

The large, temperature-independent, low-frequency dielectric constant recently observed in single-crystal $CaCu_3Ti_4O_{12}$ is most plausibly interpreted as arising from spatial inhomogenities of its local dielectric response. Probable sources of inhomogeneity are the various domain boundaries endemic in such materials: twin, Ca-ordering, and antiphase boundaries. The material in and neighboring such boundaries can be insulating or conducting. We construct a decision tree for the resulting six possible morphologies, and derive or present expressions for the dielectric constant for models of each morphology. We conclude that all six morphologies can yield dielectric behavior consistent with observations and suggest further experiments to distinguish among them.

I. INTRODUCTION

The low-frequency limit ϵ_0 of the dielectric constant $\epsilon(\omega)$ of $CaCu_3Ti_4O_{12}$ (CCTO) single-crystals can be as much as 10^3 times larger than that expected by extrapolating from electron and infrared phonon contributions, approaching 10^5 and remaining constant over a broad temperature range.[1–3] With a decrease in temperature or increase in frequency, ϵ falls off, displaying Debye-like relaxation behavior with an activated relaxation rate.[2,3] Such unexpected behavior is startling scientifically and intriguing technologically and, accordingly, has attracted much attention,[4–9] including comparative studies involving its Cd counterpart, $CdCu_3Ti_4O_{12}$ (CdCTO), which apparently shows similar though less pronounced behavior in ceramic samples.[1,10]

The central question is now whether the large dielectric response is intrinsic to a perfect crystal of CCTO or extrinsic in that it originates with defects, inhomogeneities, etc., in particular samples. Based on our first-principles calculations of the structure, the phonon spectrum, and the dynamical effective charges of both CCTO (Ref. 7) and CdCTO (Ref. 8), together with the agreement of our results with experiment[3,10] and an assessment of the existing experimental facts,[1–5,10] we have argued strongly against an intrinsic interpretation, as have others on empirical grounds.[1,11,12] At issue now is the nature of the extrinsic mechanism, which we address in the present paper.

Empirically, the single-crystal samples of CCTO are known to be to be highly twinned,[1] and the transport behavior of these domains and their boundaries, as well as those of other such domains and boundaries (in both single-crystal and ceramic samples), could play a significant role in the observed low-frequency giant dielectric response, as was noted in earlier work.[1,7,11] The basic idea is that the bulk of the material is either conducting or nearly so, and that the conductivity of the entire sample is only prevented either by a failure of the conducting regions to percolate, or else by the presence of thin insulating blocking layers at the surfaces or at internal domain boundaries. The various morphologies associated with these possibilities can all be consistent with an enormous enhancement of the static dielectric constant and with a Debye-like frequency response, although there are characteristic details of the dielectric response that may help distinguish between them.

In this article, we identify and thoroughly analyze those morphologies consistent with existing experimental results for CCTO. We begin in Sec. II by listing six morphology classes, conceived from general arguments, that are associated with internal and external boundaries probably present in CCTO and may give rise to the observed dielectric response. Internal domain boundaries present in CCTO could be conducting or nonconducting, and if the former is the case, the bulk must be insulating for a large dielectric response to be possible; alternatively if the latter is the case, the bulk must be conducting. Of course, given either instance, intrinsic or electrode-induced insulating (or blocking) layers must be present at the surface if the internal conducting regions percolate through the sample, since a finite dielectric response is observed. And, if they do not percolate, blocking layers may or may not be present. After sorting out the possible morphological scenarios, the dielectric response of blocked morphologies is discussed in Sec. III. We then provide useful exact bounds on ϵ_0 in Section IV, and afterward analyze the two unblocked morphologies in detail, completing our analysis. The dielectric properties of a solid exhibiting bulk conductivity with insulating boundaries and no blocking are derived in Section V; the converse morphology is treated in Section VI. We conclude, in Section VII, that any of these six morphologies would yield dielectric responses consistent with observations,[1–3] and that existing experiments do not distinguish them. Accordingly we propose various experiments, including the use of nanoscale probes to examine the local conductivity, to discriminate among the various possibilities presented here.

We do not consider here the possibility that the ex-

trinsic behavior arises from point or line defects randomly but homogeneously distributed throughout the bulk. One such possibility would be that oxygen vacancies, common to perovskite-like oxides and which we denote V_O, are responsible. This has already been proposed by Ramirez *et al.*,[13] and they point out that a V_O concentration of order 10^{-3} would be required. If the activation energies of $(V_O)^+$ and $(V_O)^{++}$–i.e., singly- and doubly-ionized vacancies–are comparable to those in other perovskites[2,14] and if the mobilities of electrons in the conduction band are similarly comparable,[15–17] a concentration of V_O of order 10^{-3} would give rise to a dc bulk resisitivity many orders of magnitude smaller than that observed or inferred for these materials. Accordingly we have confined our attention to two-dimensional defects.

II. SIX MORPHOLOGIES

Large quasistatic dielectric constants ϵ_0 can arise in macroscopic insulators containing conducting regions approaching a percolation threshold. While this may occur in principle for a wide range of morphologies, we consider here those six which we perceive as relevant to the good single-crystal CCTO samples possessing the largest values of ϵ_0.[3] Each morphology can be decomposed into two or three broadly-defined regions: (1) domains, (2) their associated boundaries, and (3) blocking layers (if any) parallel to the electrodes. Several domain types (and therefore boundaries) are possible. In addition to twin boundaries, a necessary by-product of the observed twinning,[1,3,10] two other categories may exist, both associated with variant chemical ordering. The first arises from the fact that the Ca sublattice may occupy four possible A sites, thus making possible four differently-ordered domains and their associated domain boundaries. The second includes antiphase domain boundaries of A–A or B–B type separating domains in which the A atoms have changed registry with the B atoms within the perovskite structure. Thus, if spatial heterogeneity in the electrical response occurs in CCTO single crystals, it may be plausibly and economically associated with an intersecting set of locally planar twin, antiphase, and/or compositional-ordering domain boundaries.

While each of the boundary regions contain planar defects, their composition may differ from that of the bulk through the Gibbs adsorption phenomenon; it follows that their effective thickness may be substantial in the present context. We can thus distinguish two possibilities. The domains themselves can be conducting or insulating in the bulk. If the domains are conducting, their boundaries must be blocking, and vice versa. Impurities or oxygen deficiencies could give rise to the bulk conductivity. Alternatively, if the impurities or vacancies segregate at or near the boundaries, the bulk would be insulating and the boundaries conducting.

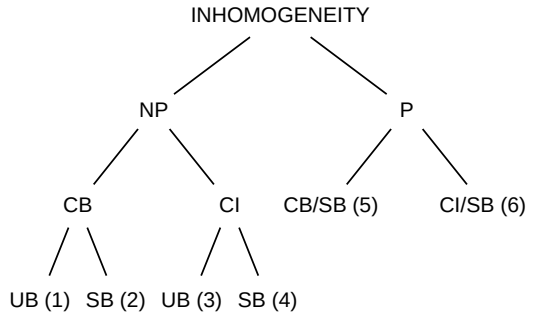

FIG. 1. Morphological decision tree showing how the possible morphological elements lead to six distinct morphologies which are nonpercolating (NP), percolating (P), conducting bulk (CB), conducting interfaces (CI), unblocked (UB), or surface blocked (SB). The numbers in parentheses correspond to those in Table I.

Conductivity may also arise at a boundary through the formation of bands of interface states, which are localized at the boundaries and extended along them, and which possess a fundamental gap signficantly smaller than the intrinsic bulk gap. This would allow the formation of shallow traps associated with the boundary imperfections. Conductivity could originate with thermally activated traps or with ordinary thermal excitation across the interfacial energy gap. For example, consider Cu-Cu antiphase boundaries. CCTO is a Mott-Hubbard insulator with an intrinsic gap of at least 1.5 eV (Ref. 3, 7). The highest valence band and lowest conduction band states are primarily *d*-orbitals hybridized with the *p*-orbitals of the four nearest-neighbor oxygens in each CuO_4 plaquette.[7] The coupling between neighboring plaquettes is weak, as evidenced by the small valence and conduction bandwidths. Within a tight-binding model, the effective Hubbard U is thus substantially larger than the effective number of neighbors z times the effective electron transfer integral t (zt is then a measure of the bandwidth within this model). However, locally, at a Cu-Cu antiphase boundary, z (and therefore the bandwidth) increases, U/zt decreases, the Hubbard gap decreases, and the possibility of boundary conductivity arises. An excess V_O concentration could also give rise to boundary conductivity as discussed further in Sec. VII.

We conclude that in the present state of our knowledge of CCTO, we must suppose that the conducting bulk (CB) and the conducting interface (CI) morphologies are equally plausible. The conducting regions can be below the percolation threshold, i.e., nonpercolating (NP), or above the percolating threshold (P). If the latter (P), conduction must be blocked by a surface barrier layer (SB). The barrier layer can be intrinsic to the surface or be associated with the electrode-CCTO interface. In the nonpercolating case, there may or may not be a blocking layer.

These possibilities can be represented by a morpho-

TABLE I. Six possible morphologies that could produce the large dielectric response.

	MORPHOLOGY	ACRONYM
1	nonpercolating, conducting bulk, unblocked	NP/CB/UB
2	nonpercolating, conducting bulk, surface blocked	NP/CB/SB
3	nonperc., conducting interfaces, unblocked	NP/CI/UB
4	nonperc., conducting interfaces, surface blocked	NP/CI/SB
5	percolating, conducting bulk, surface blocked	P/CB/SB
6	percolating, conducting interfaces, surface blocked	P/CI/SB

logical decision tree, illustrated in Fig. 1. Six distinct morphologies result, which are listed in the Table I along with the acronyms by which we identify them in the remainder of the paper.

III. BLOCKED MORPHOLOGIES

We suppose that the CCTO samples have plane-parallel boundaries normal to their smallest dimension, forming good planar electrode-sample interfaces. The effective complex dielectric constant ϵ^* for all blocked cases is then simply

$$\frac{1}{\epsilon^*} = \frac{f_{\rm L}}{\epsilon_{\rm L}} + \frac{1-f_{\rm L}}{\epsilon^*_{\rm M}}\ , \tag{1}$$

where $f_{\rm L}$ is the volume fraction of the two blocking layers which is equal to the sum of their relative thicknesses, $\epsilon_{\rm L}$ their dielectric constant (assumed to be entirely real), and $\epsilon^*_{\rm M}$ the complex macroscopic dielectric constant of the material. We now focus on two possible sample morphologies, both containing conducting regions, which lead to a large Debye-like low-frequency dielectric response; in one the conducting regions percolate, and in the other they do not.

A. Dielectric response of morphologies with percolating conducting regions

For morphologies in which the bulk material contains percolating (P) conducting regions, the frequency-dependent dielectric constant $\epsilon^*_{\rm M}$ can be expressed as

$$\epsilon^*_{\rm M} = \epsilon_{\rm M}(\omega) + 4\pi i\sigma(\omega)/\omega, \tag{2}$$

with $\epsilon^*_{\rm M}$ and $\sigma(\omega)$ real. Inserting (2) into (1) yields the Debye form

$$\epsilon^* = \epsilon_\infty + \frac{\epsilon_0 - \epsilon_\infty}{1 - i\omega\tau(\omega)}, \tag{3}$$

where

$$\epsilon_0^{-1} = \epsilon^{*-1}(\omega \to 0) = \frac{f_{\rm L}}{\epsilon_{\rm L}}, \tag{4}$$

$$\epsilon_\infty^{-1} = \epsilon^{*-1}(\omega \to \infty) = \frac{f_{\rm L}}{\epsilon_{\rm L}} + \frac{1-f_{\rm L}}{\epsilon_{\rm M}(\infty)}, \tag{5}$$

and

$$\tau(\omega) = \frac{\epsilon_0}{\epsilon_\infty}\frac{\epsilon_{\rm M}(\omega)}{4\pi\sigma(\omega)}. \tag{6}$$

In (5), $\epsilon_{\rm M}(\infty)$ is a representative value of $\epsilon_{\rm M}(\omega)$ for ω such that $\omega\tau(\omega) \gg 1$.

It follows from the above that if a percolating morphology actually occurs, it must be well beyond the percolation threshold. This results from the fact that $\epsilon_{\rm M}(0)$ diverges at the percolation threshold, so that sufficiently close to the threshold one expects no significant difference between ϵ_0 and ϵ_∞; then $\epsilon_{\rm M}(\infty) > \epsilon_0$, in direct contradiction to the observations ($\epsilon_\infty \ll \epsilon_0$).

Neglecting ϵ_∞, the asymptotic (high-frequency) behavior of the real part of ϵ^*, denoted here ϵ', is

$$\epsilon' \sim \frac{1}{\epsilon_0}\frac{[4\pi\sigma(\omega)]^2}{\omega^2}, \tag{7}$$

thus falling off with ω more slowly than the pure Debye case of ω^{-2}. Such behavior is also consistent with the experimental results of Ref. 3, and thus the two percolating blocked cases (P/SB, entries 5 and 6 of Table I), cannot be eliminated on the basis of their frequency dependence.

Using Eq. (4) with a value of $\epsilon_{\rm L} \sim 10^2$, an ϵ_0 of order 10^5 can be achieved if we take the blocking layer volume fraction as $f_{\rm L} \sim 10^{-3}$. As typical samples have thicknesses of the order of millimeters, the implied widths of the blocking layers are of the order of microns. It is unlikely, though not impossible, that barrier widths are actually that large. Moreover, values of ϵ_0 as low as 5×10^3 have been observed, implying barrier widths of the order of tens of microns, which would be improbably large. And finally, *conducting* samples have been fabricated,[18] which is inconsistent with the existence of such an electrode barrier and mitigates against the P/CB/SB and P/CI/SB cases.

In the event that a percolating morphology is demonstrated to be the most relevant to CCTO after all, a simple experiment would distinguish between intrinsic surface and electrode-induced blocking layers. Suppose an insulating film of relative thickness $f_{\rm I}/2$ and dielectric constant $\epsilon_{\rm I}$ is fabricated or deposited between each electrode and the sample. The low frequency effective dielectric constant of the composite (blocking layers plus insulating film), $\epsilon^0_{\rm eff}$, is given by

$$\frac{1}{\epsilon^0_{\rm eff}} = \frac{f_{\rm I}}{\epsilon_{\rm I}} + \frac{f_{\rm L}}{\epsilon_{\rm L}}. \tag{8}$$

An intrinsic surface blocking layer should be affected but not eliminated by the additional insulator. On the other hand, the effects of an electrode blocking layer (EB) should certainly be eliminated. Thus, measuring $1/\epsilon^0_{\rm eff}$ for values of $f_{\rm I}$ greater than the $f_{\rm L}$ for the blocking layer and then extrapolating the resulting $1/\epsilon^0_{\rm eff}$ vs. $f_{\rm I}$ towards zero $f_{\rm I}$ should yield a vanishing intercept for the EB case. A similar procedure would yield a finite intercept for the

intrinsic case, according to (8). This experiment can be carried out by depositing an electrode directly on one face of a thin CCTO sample. On the other face, a wedge of insulator is deposited followed by the deposition of a set of separated electrode strips parallel to the wedge boundary. A set of values of f_I in (10) embracing zero is thus achieved with a single sample.

B. Dielectric response of morphologies with nonpercolating conducting regions

For sample morphologies with nonpercolating conducting regions (NP), we use for ϵ_M^* the generic form

$$\epsilon_M^* = \epsilon_M^\infty + \frac{\epsilon_M^0 - \epsilon_M^\infty}{1 - i\omega\tau_M(\omega)}. \tag{9}$$

The origin of this form will be discussed in more detail for the first four cases of Table I in Secs. V and VI. Inserting (9) into (1) again yields the Debye form (3) but now with

$$\epsilon_0^{-1} = \frac{f_L}{\epsilon_L} + \frac{1 - f_L}{\epsilon_M^0}, \tag{10}$$

$$\epsilon_\infty^{-1} = \frac{f_L}{\epsilon_L} + \frac{1 - f_L}{\epsilon_M^\infty}, \tag{11}$$

and

$$\tau(\omega) = \frac{\epsilon_0}{\epsilon_\infty}\frac{\epsilon_M^\infty}{\epsilon_M^0}\tau_M(\omega). \tag{12}$$

For a value of ϵ_0 close to the observed value of approximately 10^5, it follows from Eq. (10) that f_L/ϵ_L and $(1-f_L)/\epsilon_M^0$ must be each less than 10^{-5}. Since ϵ_L should be of order 10^2, the value of ϵ_b, it follows that f_L should be 10^{-3} or less and ϵ_M^0 10^5 or larger. For a value of ϵ_∞ of approximately 10^2, it then follows from Eq. (11) that $\epsilon_M^\infty = \epsilon_\infty = 10^2$. These two results imply, with (12), that $\tau(\omega) \geq \tau_M(\omega)$.

Interposing insulating films, as in the percolating morphology in Sec. A above, should not affect the intrinsic surface barrier. This implies that

$$\frac{1}{\epsilon_{\rm eff}^0} = \frac{f_I}{\epsilon_I} + \frac{f_L}{\epsilon_L} + \frac{1 - f_I - f_L}{\epsilon_M^0} \to \frac{1}{\epsilon^0} \tag{13}$$

as $f_I \to 0$. In the electrode-induced case the barrier at the electrode is eliminated and $f_L \to 0$ so that

$$\frac{1}{\epsilon_{\rm eff}^0} = \frac{f_I}{\epsilon_I} + \frac{1 - f_I}{\epsilon_M^0} \to \frac{1}{\epsilon_M^0} \geq \frac{1}{\epsilon_0}. \tag{14}$$

In (13) and (14) the arrows signify an extrapolation to $f_I = 0$ which is carried out as described in Sec. A above. Thus, if the extrapolated value of $\epsilon_{\rm eff}^0$ exceeds ϵ_0, one learns from this experiment that the sample is blocked by an electrode-induced layer and that ϵ_M^0 exceeds ϵ_0. If $\epsilon_{\rm eff}^0$ does not exceed ϵ_0 when $f_I \to 0$, the experiment does not distinguish between the two possible sources of surface blocking.

IV. EXACT BOUNDS ON THE STATIC DIELECTRIC CONSTANT

Before discussing the nonpercolating unblocked cases (NP/CB/UB and NP/CI/UB) and, equivalently, the origin of expression (9) for ϵ_M^* in the nonpercolating blocked cases of Sec. IIIB, it is convenient to have exact bounds on the total *static* dielectric constant ϵ_0.

We make the simplification that the local dielectric and conductivity tensors are isotropic. Suppose an inhomogeneous material has a set $\{\epsilon_i\}$ of different local static dielectric constant with a corresponding set of volume fractions $\{f_i\}$. The static *macroscopic* dielectric constant ϵ_0 then lies between the exact Wiener bounds[19]

$$\left[\sum_i f_i \frac{1}{\epsilon_i}\right]^{-1} \leq \epsilon \leq \left[\sum_i f_i\, \epsilon_i\right] , \tag{15}$$

the lower bound an equality for all inhomogeneities bounded by planes parallel to the electrode planes (constant electric displacement $\mathbf{D}$) and the upper bound an equality for all inhomogeneities bounded by planes perpendicular to the electrode planes (constant electric field $\mathbf{E}$). When applied to the unblocked morphologies, these bounds are particularly illuminating, as we show below.

V. UNBLOCKED MORPHOLOGIES WITH INSULATING INTERNAL BOUNDARIES

In the absence of blocking layers, we suppose that there is a bulk volume fraction f_b with finite conductivity σ_b and a nonconducting internal interface (boundary) volume fraction $f_i = 1 - f_b$ with a finite dielectric constant ϵ_i. Since $\epsilon_b \sim 4\pi i\sigma_b/\omega \to \infty$ as $\omega \to 0$, Eq. (15) simplifies to

$$\epsilon_i/f_i \leq \epsilon \leq \infty\ . \tag{16}$$

The upper bound pertains to systems above the percolation threshold. Most interesting, however, is the lower bound; a small volume fraction $f_i \sim 10^{-3}$ associated with the interfaces and interface dielectric constant of ϵ_i comparable to ϵ_b together imply a lower bound comparable to the observed ϵ_0.

If all internal boundaries are parallel to the electrode planes, the frequency-dependent dielectric constant becomes

$$\epsilon(\omega) = \epsilon_b + \frac{\epsilon_0 - \epsilon_b}{1 - i\omega\tau(\omega)}\ , \tag{17}$$

$$\epsilon_0 = \epsilon_b/f_i\ , \tag{18}$$

$$\tau(\omega) = (1 - f_i)\epsilon_0/4\pi\sigma_b(\omega)\ ; \tag{19}$$

with $f_{\rm i}$ the volume fraction of the internal blocking layers; with the dielectric constant of the blocking layers assumed equal to $\epsilon_{\rm b}$; and with $\sigma_{\rm b}(\omega)$ the bulk conductivity within the domains. A volume fraction $f_{\rm i}$ of 10^{-3} associated with the blocking domain boundaries would account for the large observed value of ϵ_0.[3] Raevski *et al.*[18] have obtained dielectric responses similar to those of CCTO in the nonferroelectric perovskite ceramics $AFe_{1/2}B_{1/2}O_3$ with A being Ba, Sr, or Ca, and B being Nb, Ta, or Sb. They interpret their results as indicating that a Maxwell-Wagner mechanism[20] is responsible for the large permittivity and its temperature dependence, and they use a simple layered structure to illustrate their argument empirically. The layered geometry is certainly too artificial, however, as in reality CCTO is likely to possess a more complicated (and strongly nonplanar) arrangement of domains and boundaries.

A less unrealistic morphology would be spherical conducting domains surrounded by spherical shells of insulator, with $\epsilon(\omega)$ derived within the effective medium approximation.[21] The result is

$$\epsilon(\omega) = \frac{3\epsilon_c(\omega) - 2(\epsilon_c(\omega) - \epsilon_b)f_i}{3\epsilon_b + (\epsilon_c(\omega) - \epsilon_b)f_i}\epsilon_b \ , \tag{20}$$

where

$$\epsilon_c(\omega) = \epsilon_b + 4\pi i\sigma_b(\omega)/\omega \tag{21}$$

is the complex dielectric constant of the conducting domains, and we have set $\epsilon_{\rm i} = \epsilon_{\rm b}$ for simplicity. This can also be rewritten in the Debye form (17) with

$$\epsilon_0 = 3(1 - f_i)\epsilon_b/f_i \ , \tag{22}$$

$$\tau(\omega) = \epsilon_0/(1 - f_i)4\pi\sigma_b(\omega) \ . \tag{23}$$

Note that ϵ_0 is increased above the lower bound in (16) by a factor of $3(1 - f_{\rm i})$ in this morphology, according to the effective medium approximation. In both morphologies, ϵ_0 increases monotonically as $f_{\rm i}$ decreases, a feature common to all nonpercolative morphologies.

The above simple treatments lead to deviations from Debye relaxation only through the frequency dependence of $\sigma_{\rm b}(\omega)$, which may or may not be significant for these materials given our lack of understanding of the conduction mechanisms. In particular, randomness in the morphology can lead to such deviations, particularly as close to the percolation threshold as the samples appear to be, with $f_{\rm i}$ $\sim 3\times10^{-3}$ for $\epsilon_{\rm b}$ $\sim 10^2$ and ϵ_0 $\sim 10^5$. Our careful examination of the observed frequency dependence of ϵ' and ϵ'' shows that the expected deviations from Debye-like behavior are indeed present.[3] This case of conducting domains enveloped by insulating domain boundaries is identical to that of cermets with a low volume fraction of ceramic or of varistors. Since these have been exhaustively studied, we need comment no further on this case. Note that Eqs. (17), (22), and (23) provide a basis for the generic form of $\epsilon^*_{\rm M}$, Eq.(9), introduced without justification in Sec. IIIB.

VI. UNBLOCKED MOPHOLOGIES WITH CONDUCTING BOUNDARIES

In this section, we present a model of a spatially inhomegenous material whose bulk is insulating but whose internal boundary or interface regions are conducting. The model is developed from the premise that the conducting boundaries are randomly parallel to one of three orthogonal cubic planes; as a simplification, we initially treat the boundaries as disjoint disks which we further simplify to oblate ellipsoids, identical except for their random orientation, with principal axes $a = b \gg c$ and occupying volume fraction ϕ. For such a model to apply to CCTO, continuous conducting pathways through the sample formed from boundaries are forbidden, and so, while the conducting boundaries are allowed to intersect, we force the sample to be in a nonpercolating regime. The complex dielectric constant ϵ^* of our simple morphogenetic model system, derived below via an effective medium approximation, agrees quantitatively with experiments, reproducing both the magnitude and frequency-dependence of the observed dielectric response in CCTO and related materials.

We begin by supposing that our model material contains a density N of conducting boundary segments, which for simplicity we take to be in the form of disjoint thin discs of radius a' and thickness $2c'$ randomly distributed in the three cubic planes with volume fraction

$$\phi = 2\pi N a'^2 c'. \tag{24}$$

Since the overall symmetry is still cubic, we note that ϵ is a scalar, and thus the response can be computed by assuming an electric field and polarization parallel to a single cubic axis. We now derive ϵ^* via an effective-medium approximation. Suppose that each disc is at the center of a sphere of radius b of the bulk material with complex susceptibility $\chi_{\rm b}$, where

$$\epsilon_{\rm b} = 1 + 4\pi\chi_{\rm b}, \tag{25}$$

outside of which is the effective medium. The volume fraction within the sphere of bulk material then becomes

$$\phi = \frac{3}{2}\frac{a'^2 c'}{b^3} \ , \tag{26}$$

which leads to an important condition: for the conducting discs to contain the spheres completely and therefore be below the percolation threshold, we must have $\frac{2}{3}\frac{a'}{c'}\phi < 1$ in order to make contact with experiments.

A. Bulk polarization

The total macroscopic polarization contains contributions from the bulk-like insulating domains, and also their associated internal conducting interfaces. We derive each contribution in turn. The polarization in the

bulk material, $P_{\rm b}$, is related to the local field within the bulk, $E_{\rm b}^{\rm loc}$, as

$$P_{\rm b} = \chi_{\rm b} E_{\rm b}^{\rm loc} \; ; \tag{27}$$

the local field inside the bulk material can be expressed in terms of local and macroscopic polarizations, and also the macroscopic field, as

$$E_{\rm b}^{\rm loc} = E_{\rm mac} + \frac{4\pi}{3}(P_{\rm mac} - P_{\rm b}) \; , \tag{28}$$

where $E_{\rm mac}$ is the macroscopic field in the effective medium and $P_{\rm mac}$ is given by

$$P_{\rm mac} = \chi_{\rm mac}^{*} \, E_{\rm mac} = \frac{\epsilon^{*} - 1}{4\pi} E_{\rm mac} \; , \tag{29}$$

where

$$\epsilon^{*} = 1 + 4\pi \chi_{\rm mac}^{*} \; . \tag{30}$$

To obtain ϵ^{*}, we need an expression for the macroscopic polarization, $P_{\rm mac}$, in terms of $E_{\rm mac}$. We begin by first obtaining the former, $P_{\rm b}$, in terms of $E_{\rm mac}$. Inserting (29) into (28) gives

$$E_{\rm b}^{\rm loc} = \frac{\epsilon^{*} + 2}{3} E_{\rm mac} - \frac{4\pi}{3} P_{\rm b} \; ; \tag{31}$$

now, inserting (31) into (27), we obtain the desired result

$$P_{\rm b} = \frac{\frac{1}{3}(\epsilon^{*} + 2)\chi_{\rm b}}{1 + \frac{4\pi}{3}\chi_{\rm b}} E_{\rm mac} \; . \tag{32}$$

B. Polarization of the conducting internal interfaces

Deriving the conducting-interface contribution to the macroscopic polarization is slightly more involved, and, to simplify the discussion without loss of generality, we now replace conducting discs with ellipsoids of the same volume $4\pi a^2 c/3 = 2\pi a'^2 c'$ and the same eccentricity

$$e = \sqrt{\left(\frac{a}{c}\right)^2 - 1} = \sqrt{\left(\frac{a'}{c'}\right)^2 - 1} >> 1, \tag{33}$$

where $a = (3/2)^{1/3} a'$, so that the polarization and electrostatic field inside remain uniform. The volume fraction of ellipsoids to bulk material (Eq. (26)) then becomes

$$\phi = \frac{a^2 c}{b^3}. \tag{34}$$

The local field $E_{\alpha i}^{\rm loc}$ inside the ellipsoid differs from $E_{\rm b}^{\rm loc}$ by the depolarizing field introduced by the surface charge arising from the change in polarization across the the ellipsoid-bulk interface:

$$E_{\alpha i}^{\rm loc} = E_{\rm b}^{\rm loc} + L_{\alpha}(P_{\rm b} - P_{\alpha i}) \; , \tag{35}$$

where $P_{\alpha i}$ is the polarization inside, L_{α} is the depolarization factor, and α specifies the cubic axess normal to the boundary plane, i.e., normal to the semi-minor axis c, where $\sum_{\alpha} L_{\alpha} = 4\pi$. Using the linear relation $P_{\alpha {\rm i}} = \chi_{\rm i}^{*} E_{\alpha i}^{\rm loc}$, and also Eq. (35), we find

$$P_{\alpha {\rm i}} = \frac{\chi_{\rm i}^{*}(1 + L_{\alpha}\chi_{\rm b})}{1 + L_{\alpha}\chi_{\rm i}^{*}} E_{\rm b}^{\rm loc}, \tag{36}$$

where

$$\chi_{\rm i}^{*} = \chi_{\rm b} + \frac{i\sigma_{\rm i}}{\omega} \tag{37}$$

is the complex susceptibility of the boundary region, $\sigma_{\rm i}$ its conductivity, and the real part of $\chi_{\rm i}^{*}$ has been taken as $\chi_{\rm b}$ for simplicity. Using (31) and (32), $E_{\rm b}^{\rm loc}$ can be expressed in terms of $E_{\rm mac}$ as

$$E_{\rm b}^{\rm loc} = \frac{\frac{1}{3}(\epsilon^{*} + 2) E_{\rm mac}}{1 + \frac{4\pi}{3}\chi_{\rm b}}; \tag{38}$$

and from (36) and (38), we relate $P_{\alpha {\rm i}}$ and $E_{\rm mac}$, as desired:

$$P_{\alpha {\rm i}} = \frac{1}{3}(\epsilon + 2) \frac{\chi_{\rm i}^{*}(1 + L_{\alpha}\chi_{\rm b})}{1 + L_{\alpha}\chi_{\rm i}^{*}} \frac{E_{\rm mac}}{1 + \frac{4\pi}{3}\chi_{\rm b}} \; . \tag{39}$$

We now impose the effective-medium self-consistency condition that $P_{\rm mac}$ is the volumetric average of $P_{\rm b}$, i.e.,

$$P_{\rm mac} = (1 - \phi) P_{\rm b} + \phi P_i \; , \tag{40}$$

where we have taken the orientational average $P_i = \frac{1}{3}\sum_{\alpha} P_{\alpha i}$. The above equation, with the values of $P_{\alpha i}$ and $P_{\rm b}$ derived above, expresses $P_{\rm mac}$ linearly in terms of $E_{\rm mac}$.

C. Dielectric response

We now recast $\epsilon^{*} = 1 + 4\pi P_{\rm mac}/E_{\rm mac}$ in the suggestive form

$$\epsilon^{*} = \frac{\epsilon_{\rm b} + \frac{8\pi}{3} B_{\rm i} \phi}{1 - \frac{4\pi}{3} B_{\rm i} \phi} \; , \tag{41}$$

where we define

$$B_{\rm i} = \frac{1}{3} \sum_{\alpha} \frac{1}{L_{\alpha}} \frac{1}{1 - i\omega\tau_{\alpha}} \tag{42}$$

and

$$\tau_{\alpha} = \left(\frac{1}{L_{\alpha}} + \chi_{\rm b}\right) \frac{1}{\sigma_i}. \tag{43}$$

The quantities $B_{\rm i}$ can be thought of as inverse depolarization factors, with an additional dynamical correction.

Equation (41) is a generalization of the Clausius-Mossotti relation which displays the proper limiting behavior, as follows. First, ϵ reduces to $\epsilon_{\rm b}$ when ϕ vanishes. Second, it reduces to the Clausius-Mossotti relation in standard form for an array of metallic spheres for which $\chi_{\rm b} = 0$, $B_{\rm i} \to 3/4\pi$ as $\omega \to 0$; that is,

$$\epsilon = \frac{1 + \frac{8\pi}{3} N\alpha}{1 - \frac{4\pi}{3} N\alpha}. \tag{44}$$

where $\alpha = a^3$ is the polarizability for the case that $c = a$. Third, when $\sigma_{\rm i} \to 0$, the material becomes uniform and ϵ^* reduces to $\epsilon_{\rm b}$.

In the present case, $\rm B_i$ is the sum of two terms and can be written explicitly as

$$B_{\rm i} = \frac{2}{3}\frac{1}{L_a}\frac{1}{1 - i\omega\tau_a} + \frac{1}{3}\frac{1}{L_c}\frac{1}{1 - i\omega\tau_c} = B_a + B_c, \tag{45}$$

where B_a and B_c are associated with the semimajor axes a and c, and

$$\tau_a = (\chi_{\rm b} + 1/L_a)/\sigma_{\rm i} \tag{46}$$

and

$$\tau_c = (\chi_{\rm b} + 1/L_c)/\sigma_{\rm i}. \tag{47}$$

From Landau and Lifshitz,[22] we obtain

$$L_c = 4\pi\frac{1 + e^2}{e^3}(e - \tan^{-1} e)\ , \tag{48}$$

$$L_a = \frac{1}{2}(4\pi - L_c)\ , \tag{49}$$

with e given by (33). For the oblate ellipsoids, a/c and e are large enough so that L_c approaches 4π and L_a becomes small,

$$L_a = \pi^2\frac{c}{a}. \tag{50}$$

Inserting $L_c = 4\pi$ and (50) for $\rm L_a$ into (45) and (46) yields

$$B_a = \frac{2}{3\pi^2}\frac{a}{c}\frac{1}{1 - i\omega\tau_a} \tag{51}$$

and

$$B_c = \frac{1}{12\pi}\frac{1}{1 - i\omega\tau_c}, \tag{52}$$

with

$$\tau_a = \frac{\frac{4}{\pi}\frac{a}{c} + \epsilon_{\rm b} + 1}{4\pi\sigma_{\rm i}} \tag{53}$$

and

$$\tau_{\rm b} = \frac{\epsilon_{\rm b}}{4\pi\sigma_{\rm i}}. \tag{54}$$

B_a and B_c assume their maximum magnitudes at $\omega = 0$; explicitly,

$$B_a(0) = \frac{2}{3\pi^2}\frac{a}{c} \gg B_c(0) = \frac{1}{12\pi} \tag{55}$$

provided $a/c \gg 1$. Since $\phi \ll 0$ and $\epsilon_{\rm b} \sim$ 80-90 (Refs. 3, 7), $(8\pi/3)B_c(0)\phi$ is negligible relative to $\epsilon_{\rm b}$ in the numerator of ϵ^*, (41), and $(4\pi/3)B_c(0)\phi$ is negligible compared with unity in the denominator of ϵ^*. From (51), the ratio of the relaxation times is

$$\frac{\tau_a}{\tau_{\rm b}} = \frac{4}{\pi}\frac{a}{\epsilon_{\rm b}c} + 1 - \frac{1}{\epsilon_{\rm b}}. \tag{56}$$

Under the suppositions that $a \gg c$ and $\phi \ll 1$, it can be shown from (51), (53), and (56) that $\rm B_c$ does not contribute significantly to ϵ^* at any frequency, independent of the relative magnitudes of a/c and $\epsilon_{\rm b}$ in (56).

$\rm B_c$ can thus be safely neglected, and ϵ^* can be put into the Debye form with $\epsilon_\infty = \epsilon_{\rm b}$ and

$$\epsilon_0 = \frac{\epsilon_{\rm b} + \frac{8\pi}{3} N\bar{a}^3}{1 - \frac{4\pi}{3} N\bar{a}^3}. \tag{57}$$

Remarkably, Eq. (57) allows the dielectric constant to be interpreted as that arising from a collection of metallic spheres of effective radius

$$\bar{a} = \left(\frac{8}{9\pi}\right)^{1/3} a \cong \frac{2}{3}a \tag{58}$$

embedded in a medium of dielectric constant $\epsilon_{\rm b}$.

Equation (57) can be rewritten as

$$\epsilon_0 = \frac{\epsilon_{\rm b} + 2\bar{f}}{1 - \bar{f}}, \tag{59}$$

where

$$\bar{f} = \frac{4\pi}{3} N\bar{a}^3 \tag{60}$$

is the volume fraction of the regions of the sample within which the electrostatic field is screened out by the a-oriented conducting boundaries, an analogue of the Faraday cage effect. The Debye relaxation time is now given by

$$\tau = \frac{\tau_{\rm a}}{1 - \bar{f}}. \tag{61}$$

As for Eq. (23) for the NP/CB/UB case, all temperature and frequency dependence of τ arises from the conductivity $\sigma_{\rm i}$.

There is a pseudo percolation threshold at $\bar{f} = 1$ at which ϵ in Eq. (59) diverges when the field-free regions percolate. However, this mean-field theory and the geometry of the model both grossly overestimate the value of the percolation threshold through neglect of randomness.[19] This overestimated threshold occurs at a value of ϕ about 1.5% below the true percolation threshold of our disk-in-a-sphere model when the disk and sphere radii coincide, also overestimated.

VII. DISCUSSION AND CONCLUSIONS

We have constructed six possible morphologies for inhomogeneity in the local dielectric response of CCTO by supposing the properties of the internal boundary regions to be opposite from those of the bulk. (If one conducts, the other is insulating, and vice versa.) We have pointed out that the large dielectric constants result either when the conducting regions almost percolate or when they percolate but are blocked at the surface or electrode interface. We have analyzed the expected dielectric properties of all six morphologies in Secs. III-VI, in some cases explicitly and in others by model calculation. Without exception, the dielectric properties of each of the six morphologies can be consistent with all reported observations.[1–3] Our principal conclusion is that existing experiments do not distinguish between grossly different morphologies, e.g., conducting bulk inhibited from percolation by insulating internal boundaries, and conducting internal boundaries embedded in and disrupted by insulating bulk. As discussed in Sec. III, distinguishing between intrinsic and electrode-induced surface barriers can be achieved by studying the dielectric response as a function of the thicknesses of insulating layers interposed between the CCTO sample and electrodes. However, the central questions are about the morphology of the conducting regions: are they bulk or are they associated with specific internal 2D faults? The nonlinear current-voltage characteristics of the two morpholgies should differ quantitatively. In both cases there should be a threshold field at which current rises rapidly with voltage, going over to a superlinear voltage dependence. In the conducting boundary morphology (case 3), field concentration would occur at the breaks in the current pathways along the boundaries; this would not occur if the bulk were conducting (case 2), and thus its threshold voltage would be higher.

Additional dielectric measurements at low frequencies (<1 MHz) and temperatures (T<100 K) may be able to distinguish morphologies with conducting bulk (CB) from those with conducting boundaries or interfaces (CI). According to Homes *et al.*,[3] the *intrinsic* bulk dielectric constant ϵ_0 is enhanced by about 75% as the temperature is reduced to 10 K from room temperature, a surprising increase which can be linked mainly to an increase in oscillator strength of one low-frequency IR-active mode.[3] This temperature dependence would carry over to the extrinsic giant dielectric response in CI cases, since in these scenarios the giant response comes about from an amplification of the bulk ϵ_0. In CB morphologies, however, the intrinisic boundary ϵ_0 may or may not be different from that of the bulk, and would not necessarily exhibit a temperature dependence. Thus, if measurements of the giant response at low temperatures (and lower frequencies) did not show the increase expected from that of the bulk ϵ_0, one could infer that the CI morphologies do not occur and that in the CB morphologies the boundary ϵ_0 differs significantly in its temperature dependence from that of the bulk. In addition, we note in both the CCTO and Cd-CTO ϵ_0 increases dramatically at higher temperatures. This would follow directly from a thermally-stimulated increase in conductivity locally throughout the material, bringing it closer to the perocolation threshold. However, such would be the case for all morphologies and, accordingly, is not diagnostic.

Additionally, what is the mechanism responsible for the conductivity? The observed activation energy of the relaxation time τ is that of the conductivity. The values obtained are consistent with extrinsic conductivity associated with shallow traps. It would be of interest to inject charge at one interface and measure the distribution of arrival times at the other to see whether anomalous transport occurs.

Observations with probes sensitive to the conductivity, structure, and composition at the nanoscale would be of significant experimental interest. In Sec. II we discussed a possible mechanism by which conductivity might arise in a Cu-Cu antiphase boundary. In (Ba,Sr)TiO_3 A-A and B-B antiphase boundaries, Naumov *et al.*[23] have found compressive stress via first-principles computations. This could be relaxed by a locally increased concentration of oxygen vacancies leading to activated n-type conduction in the boundaries, as discussed in Sec. I for vacancies in the bulk. Measurements of the sign of the thermopower of samples with measureable conductivities could therefore be interesting. However, one should recognize that the conducting boundary morphologies require fine tuning of the boundary volume fraction to remain close but not exceed the percolation threshold.

Finally it is important to recognize that the mechanisms leading to large dielectric constants can differ in polycrystalline (ceramic) and single-crystal samples. For the former, a model of conducting grains and blocking grain boundaries may be the most plausible since, if the reverse were true, the grain boundaries would percolate and there would be substantial conductivity. For the latter, we cannot yet distinguish between conducting and insulating internal boundaries. Tselev *et al.*,[24] however, have argued for the conducting bulk and insulating internal boundary morphology, the conductivity being associated with oxygen vacancies and the insulating boundaries being deficient in oxygen vacancies.

ACKNOWLEDGMENTS

This work was supported by NSF Grant DMR-9981193 and by the Center for Piezoelectric Design (CPD) under ONR grant N0001401-1-0365. We would like to thank I. Naumov, K. M. Rabe, and A. Tselev for providing results prior to publication.

[1] M. A. Subramanian, D. Li, N. Duan, B. A. Reisner, and A. W. Sleight, J. Solid State Chem. **151**, 323 (2000).
[2] A. P. Ramirez, M. A. Subramanian, M. Gardel, G. Blumberg, D. Li, T. Vogt, and S. M. Shapiro, Solid State Commun. **115**, 217 (2000).
[3] C. C. Homes, T. Vogt, S. M. Shapiro, S. Wakimoto, and A. P. Ramirez, Science **293**, 673 (2001).
[4] A. Koitzsch, G. Blumberg, A. Gozar, B. Dennis, A. P. Ramirez, S. Trebst, and S. Wakimoto, Phys. Rev. B **65**, 052406 (2002).
[5] Y. J. Kim, S. Wakimoto, S. M. Shapiro, P. M. Gehring, and A. P. Ramirez, Solid State Commun. **121**, 625 (2002).
[6] W. Si, E. M. Cruz, P. D. Johnson, P. W. Barnes, P. Woodward, and A. P. Ramirez, Appl. Phys. Lett. **81**, 2056 (2002).
[7] L. He, J. B. Neaton, M. H. Cohen, D. Vanderbilt, and C. C. Homes, Phys. Rev. B **65**, 214112 (2002).
[8] L. He, J. B. Neaton, D. Vanderbilt, and M. H. Cohen, Phys. Rev. B **67**, 012103 (2003).
[9] M. D. Johannes, W. E. Pickett, and R. Weht, Mat. Res. Soc. Sym. **718**, 25 (2002).
[10] C. C. Homes, T. Vogt, S. M. Shapiro, W. Wakimoto, M. A. Subramanian, and A. Ramirez (unpublished).
[11] D. C. Sinclair, T. A. Adams, F. D. Morrison, and A. R. West, Appl. Phys. Lett. **80**, 2153 (2002).
[12] P. Lunkenheimer, V. Bobnar, A. V. Pronin, A. I. Ritus, A. A. Volkov, and A. Loidl, Phys. Rev. B **66**, 052105 (2002).
[13] A. P. Ramirez, G. Lawes, V. Butko, M. A. Subramanian, and C. M. Varma, cond-mat/0209498 (unpublished).
[14] D. M. Smyth, Prog. Solid State Chem. **15**, 145 (1984).
[15] H. Ihrig and D. Hennings, Phys. Rev. B **17**, 4593 (1978).
[16] S. H. Wemple, Phys. Rev. **137**, A1575 (1965).
[17] P. Bernasconi, I. Biaggio, M. Zgonik, and P. Günter, Phys. Rev. Lett. **78**, 106 (1997).
[18] I. P. Raevski, S. A. Prosandeev, A. S. Bogatin, M. A. Malitskaya, and L. Jastrabik, J. Appl. Phys. **93**, 4130 (2003).
[19] S. Torquato, *Random Heterogeneous Materials: Microstructure and Macroscopic properties*, (Springer, New York, 2002), p. 556.
[20] *Ibid.*, pp. 460ff. We note that Maxwell approximations are not self-consistent.
[21] *Ibid.*, p. 463.
[22] L. D. Landau and E. M. Lifschitz, *Electrodynamics of Continuous Media*, Vol. 8, (Pergamon Press, Oxford, 1975), pp. 27,44.
[23] I. Naumov, K. M. Rabe, and M. H. Cohen (unpublished).
[24] A. Tselev, C. Brooks, H. Zheng, L. Salamanca-Riba, S. Anlage, R. Ramesh, and M. A. Subramanian (unpublished).